# Numerical Model for Turbulent Jets Impinging on a Surface with Throughflow

S. Polat,* A. S. Mujumdar,† A. R. P. van Heiningen,‡ and W. J. M. Douglas†
*McGill University, Montreal, H3A 2A7 Canada*

**Flow and heat transfer under confined turbulent impinging slot jets were predicted by solving iteratively the two-dimensional Navier-Stokes, energy, and turbulence model equations. The turbulence model was the high-Reynolds-number version of the well-known $k$-$\epsilon$ model. Recent work has shown that a modification of the Chieng-Launder-type near-wall model gives better agreement with measurements at small nozzle-to-surface spacings, $H/w \leq 2.6$. The predictive capability of this model was therefore tested for the effects of nozzle-exit turbulence and of impingement surface throughflow for a single jet and for the industrially important system of confined multiple jets with symmetrical exhaust ports, with and without throughflow. The model underpredicts the enhancement of heat transfer with increasing nozzle-exit turbulence but accurately predicts the effect of impingement surface throughflow for throughflow velocities less than 0.1 m/s. Heat transfer under multiple jets was predicted within 30% of the experiments.**

## Nomenclature

$A, B$ = constants of the equation for wall shear stress with throughflow
$C_1, C_2, C_\mu$ = turbulence model constants, Table 1
$E$ = a constant in the log law of the wall, Table 2
$G$ = turbulence kinetic energy generation, Table 1
$G_{P,w}$ = turbulent kinetic energy at near-wall node
$H$ = nozzle-to-impingement surface spacing, mm
$h$ = nondimensional enthalpy; $h_{con}$, at the confinement surface; $h_{imp}$, at the impingement surface
$I_j$ = turbulence intensity at jet nozzle exit
$k$ = turbulence kinetic energy, $m^2/s^2$
$k_v$ = turbulent kinetic energy at the edge of viscous sublayer
$k_P$ = turbulence kinetic energy at near-wall node
$Mu_s$ = throughflow prameter, $= u_s/u_j$
$Nu$ = Nusselt number, with characteristic dimension, $= w$
$NX$ = number of grid lines in $x$ direction
$NY$ = number of grid lines in $y$ direction
$p$ = static pressure, Pa
$\dot{q}_w$ = heat flux at wall, W
$Re$ = Reynolds number
$S_\phi$ = source term in Eq. (1)
$St$ = Stanton number with characteristic dimension, $= w$
$u$ = velocity in $x$ direction, m/s
$u_j$ = velocity at jet nozzle exit, m/s
$u_s$ = throughflow velocity, m/s
$v$ = velocity in $y$ direction, m/s
$v^+$ = nondimensional velocity, $= v/v_\tau$
$v_\tau$ = friction velocity, $= \tau_w/\rho C_\mu^{1/4} k_P^{1/2}$
$w$ = nozzle width, mm
$x$ = coordinate normal to impingement surface, m
$x^+$ = nondimensional distance from wall, Table 2
$x_v$ = distance from wall to edge of viscous sublayer, m
$\Delta x$ = distance between finite-difference layers in $x$ direction, m
$y$ = coordinate parallel to impingement surface, m
$\Delta y$ = distance between finite-difference layers in $y$ direction, m
$\Gamma_\phi$ = transfer coefficient associated with $\phi$, Eq. (1)
$\epsilon$ = dissipation of turbulent kinetic energy, $m^2/s^3$
$\kappa$ = von Kármán constant, Table 2
$\mu$ = dynamic viscosity, Pa·s
$\mu_{eff}$ = effective viscosity, $\mu_L + \mu_T$, Pa·s
$\mu_L$ = laminar viscosity, Pa·s
$\mu_T$ = turbulent viscosity, Pa·s
$\nu$ = kinematic viscosity, $m^2/s$
$\rho$ = density, $kg/m^3$
$\sigma_k$ = turbulence model constant, Table 1
$\sigma_L$ = laminar Prandtl number, = 0.7
$\sigma_T$ = turbulent Prandtl number, Table 1
$\sigma_\epsilon$ = turbulence model constant, Table 1
$\tau_w$ = wall shear stress, Pa
$\phi$ = general variable, Eq. (1)

## Introduction

THE design of an impinging jet system for a given thermal application requires the specification of a large number of geometric and flow parameters, e.g., jet-type (round/slot), jet-exhaust configuration, nozzle-to-impingement surface spacing, nozzle-to-nozzle spacing, jet confinement hood, and jet Reynolds number. Additional important effects, depending on the application, include nozzle geometry, induced or imposed crossflow, large jet-to-impingement surface temperature difference, moving impingement surface, mass transfer, or throughflow or blowing at the impingement surface. With this impressive number of design parameters, an advantageous strategy is the use of complementary numerical and experimental studies of transport processes under impinging jets.

An iterative solution of the exact transport equations for turbulent flows is currently limited by computer capacity since the small scale of turbulence requires an unrealistically large number of grids in the flow domain. An alternative is the use of a model to predict the turbulence quantities that appear in the time-averaged transport equations for turbulent flows. For the complex flow structure under impinging jets, earlier one-equation models of turbulence have been replaced by higher-

Received May 15, 1989; revision received Nov. 6, 1989; accepted for publication Jan. 17, 1990. 

*Research Associate, Department of Chemical Engineering, Pulp and Paper Research Centre; currently Winton Hill Technical Center, Procter and Gamble Company, Cincinnati, OH.

†Professor, Department of Chemical Engineering, Pulp and Paper Research Centre.

‡Associate Scientist, Department of Chemical Engineering, Pulp and Paper Research Centre.

order models that solve transport equations for various turbulence quantities, i.e., turbulent kinetic energy, turbulent kinetic energy dissipation, or individual Reynolds stresses. The high-Reynolds-number version of the $k$-$\epsilon$ turbulence model[1-6] is preferred for impingement systems. The prediction of impingement heat transfer by van der Meer[7] with an anisotropy model and by Looney and Walsh[8] with the algebraic stress models of Rodi[9] and Ljuboja and Rodi[10] as well as with the high-*Re* $k$-$\epsilon$ model indicated that these higher models do not improve predictions. The $k$-$\epsilon$ model retains a reasonable combination of economy and accuracy even for the complex configuration of impingement flows.

A recent review by Polat et al.[11] indicated that for heat and mass transfer rates under impinging jets, an aspect of great engineering interest, the numerous studies with predictions and measurements differ substantially. When a high-*Re* turbulence predictive model is employed, the requirement of a separate model to treat the near-wall boundary provides a further source of error. Discrepancies may then derive from either the turbulence model or the near-wall model. The effect of near-wall modeling on impingement heat transfer was reported by Amano and Sugiyama[12] and Polat[13] for round and slot jets, respectively.

For single and multiple confined turbulent plane jets, the present study predicts heat transfer rates along the impingement surface by solution of the two-dimensional Navier-Stokes, energy, and turbulence model equations using an upwind finite-difference scheme.[14] The turbulence model used was the high-*Re* version of the $k$-$\epsilon$ model. Polat[13] showed that, of the various near-wall models tested, a modified version of the two-layer model of Chieng and Launder[15] gives better overall agreement between prediction and measurement at low values of nozzle-to-surface spacing, $H/w$, where prediction is most difficult. One objective of the present study is to test the predictive capability of this model regarding the effects of two important parameters: nozzle-exit turbulence and surface throughflow. The second objective is to predict with this model an industrially important configuration of confined multiple impinging jets with symmetrical exhaust ports with and without throughflow.

## Mathematical Formulation of the Problem

The generalized governing equation, including continuity, is

$$\frac{\partial(\rho u\Phi)}{\partial x}+\frac{\partial(\rho v\Phi)}{\partial y}=\frac{\partial}{\partial x}\left(\Gamma_\Phi\frac{\partial\Phi}{\partial x}\right)+\frac{\partial}{\partial y}\left(\Gamma_\Phi\frac{\partial\Phi}{\partial y}\right)+S_\Phi \quad (1)$$

where $\Phi$ represents the variables $u$, $v$, $h$, $k$, and $\epsilon$. The variable $\Gamma_\Phi$ is the transfer coefficient associated with $\Phi$, and $S_\Phi$ is the corresponding source term. To express the governing equation of a particular variable in this generalized form, terms other than those in the form of "convection" and "diffusion" terms are collected in the source term $S_\Phi$. The terms $\Gamma_\Phi$ and $S_\Phi$ are shown in Table 1. As turbulent viscosity $\mu_T$ is determined by flow conditions, it must be modeled in terms of measurable flow quantities. For this the two-equation $k$-$\epsilon$ turbulence model of Jones and Launder[16] is used.

In the $k$-$\epsilon$ model $\mu_T$ is related to the turbulence terms $k$ and $\epsilon$ as

$$\mu_T = C_\mu \rho k^2/\epsilon \quad (2)$$

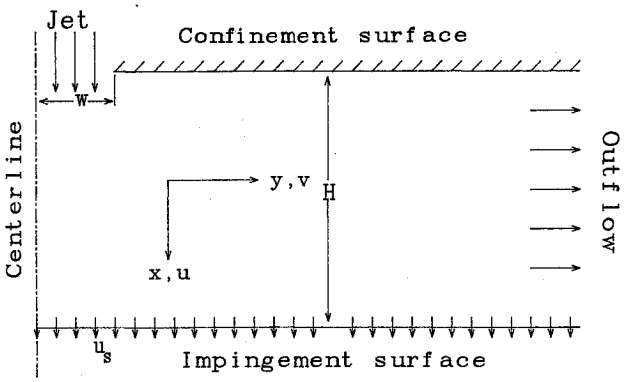


**Fig. 1 Flow configuration for a single impinging jet.**

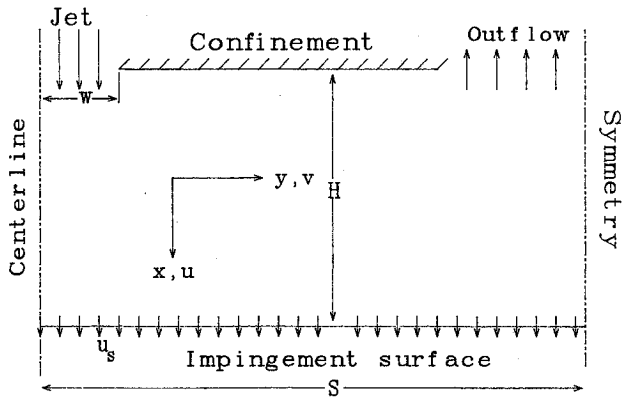


**Fig. 2 Flow configuration for multiple impinging jets.**

**Table 1 Summary of the equations solved**

| Equation | $\Phi$ | $\Gamma_\Phi$ | $S_\Phi$ |
|---|---|---|---|
| Continuity | 1 | 0 | 0 |
| $x$ Momentum | $u$ | $\mu_L+\mu_T$ | $-\frac{\partial p}{\partial x}+\frac{\partial}{\partial x}\left[(\mu_L+\mu_T)\frac{\partial u}{\partial x}\right]+\frac{\partial}{\partial y}\left[(\mu_L+\mu_T)\frac{\partial v}{\partial x}\right]$ |
| $y$ Momentum | $v$ | $\mu_L+\mu_T$ | $-\frac{\partial p}{\partial y}+\frac{\partial}{\partial x}\left[(\mu_L+\mu_T)\frac{\partial u}{\partial y}\right]+\frac{\partial}{\partial y}\left[(\mu_L+\mu_T)\frac{\partial v}{\partial y}\right]$ |
| Energy | $h$ | $\frac{\mu_L}{\sigma_L}+\frac{\mu_T}{\sigma_T}$ | 0 |
| Turbulent energy | $k$ | $\mu_L+\frac{\mu_L}{\sigma_k}$ | $G-\rho\epsilon$ |
| Turbulence energy dissipation | $\epsilon$ | $\mu_L+\frac{\mu_L}{\sigma_\epsilon}$ | $C_1\frac{\rho\epsilon}{k}G-C_2\frac{\rho\epsilon^2}{k}$ |

where $G\equiv\mu_T\left\{\left(\frac{\partial u}{\partial y}+\frac{\partial v}{\partial x}\right)^2+2\left[\left(\frac{\partial u}{\partial x}\right)^2+\left(\frac{\partial v}{\partial y}\right)^2\right]\right\}$

$C_\mu = 0.09$; $C_1 = 1.43$; $C_2 = 1.92$; $\sigma_K = 1.0$; $\sigma_\epsilon = 1.3$; $\sigma_T = 0.9$

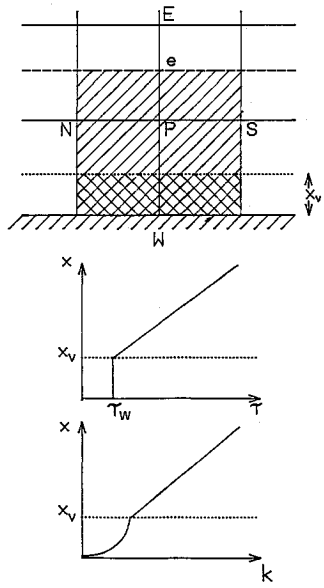


**Fig. 3 Near-wall model.**

The transport equations for turbulent kinetic energy $k$ and its dissipation rate $\epsilon$ are summarized in Table 1.

**Boundary Conditions in the Flows**

For the two flow configurations (Figs. 1 and 2), the boundary conditions include the following.

1) Nozzle exit: Uniform nozzle-exit profiles for velocity $u_j$ and nondimensional enthalpy, $h_j = 1$.

Boundary conditions for $v$, $k$, and $\epsilon$ are

$$v_j = 0 \qquad k_j = I_j^2 u_j^2; \qquad \epsilon_j = C_\mu k_j^{3/2} / \left(0.03 \frac{w}{2}\right)$$

2) Symmetry axes:

$$v = \frac{\partial u}{\partial y} = \frac{\partial k}{\partial y} = \frac{\partial \epsilon}{\partial y} = \frac{\partial h}{\partial y} = 0$$

3) Outflow for a single impinging jet:

$$u = \frac{\partial v}{\partial y} = \frac{\partial k}{\partial y} = \frac{\partial \epsilon}{\partial y} = \frac{\partial h}{\partial y} = 0$$

and for multiple impinging jets:

$$v = \frac{\partial k}{\partial x} = \frac{\partial \epsilon}{\partial x} = \frac{\partial h}{\partial x} = 0$$

and $u = u_{\text{out}}$, a uniform velocity calculated from the overall mass balance. Exhaust port width is twice the nozzle width.

**Boundary Conditions at the Impingement and Confinement Surfaces**

The confinement and impingement surface conditions are

$$u = 0 \quad \text{or} \quad u_s; \quad v = 0; \quad h_{\text{con}} = 1; \quad h_{\text{imp}} = 0; \quad k = \epsilon = 0$$

*Definition of Near-Wall Flow Region*

The high-*Re* version of the $k$-$\epsilon$ model of turbulence implies a negligible effect of viscosity on the energy containing motions and a negligible effect of the mean strain field on the dissipative ones. Although valid in most of the flow domain, in the immediate vicinity of the impingement and confinement surfaces, direct viscous effects are influential due to the no-slip condition. This very thin viscosity-affected flow region must be handled separately due to turbulence model requirements. Boundary conditions are therefore specified not at the wall but at the nodes closest to the wall. With the high-*Re* turbulence model, the first grid line must be sufficiently far from the wall to be within the fully turbulent regime, whereas the intermediate flow is handled by a near-wall model. The general concept of the present near-wall model was introduced by Chieng and Launder.[15] In this model the near-wall flow is considered viscous in the viscous sublayer and fully turbulent beyond this point. The thickness of the viscous sublayer is calculated assuming the value of the dimensionless distance from the wall $x^+$ is constant and equal to 11.5 at the edge of this layer, $x_v = 11.5\mu_L / C_\mu^{1/4} \rho k_v^{1/2}$.

*Generation of Turbulent Kinetic Energy*

It is assumed that the turbulent shear stress, zero within the viscous sublayer, undergoes an abrupt increase at the edge of the sublayer, thereafter increasing linearly (Fig. 3). The precise form of this linear variation is obtained by connecting the turbulent shear stress at the outer edge of the cell $\tau_e$ with the wall shear stress $\tau_w$. Since there is no turbulence generation in the viscous sublayer, $G_{P,w}$ is evaluated as

$$G_{P,w} = \left\{ \frac{1}{x_e} \int_{x_v}^{x_e} \left[ \tau_w + (\tau_e - \tau_w) \frac{x}{x_e} \right] \left( \frac{\partial v}{\partial x} + \frac{\partial u}{\partial y} \right) \mathrm{d}x \right\} \Delta y_{ns} + \int_v \int 2\mu_T \left[ \left( \frac{\partial u}{\partial x} \right)^2 + \left( \frac{\partial v}{\partial y} \right)^2 \right] \mathrm{d}x \, \mathrm{d}y$$

To obtain the Table 2 equation for $G_{P,w}$, this equation is integrated by using the expression $v = \tau_w \ell n(Ex^+)/\kappa \rho C_\mu^{1/4} k^{1/2}$ to calculate $\partial v / \partial x$. In the $G_{P,w}$ equation, $k_v$ is used as the approximate average $k$ in the cell.

*Dissipation of Turbulent Kinetic Energy*

The dissipation rate of turbulence energy in the viscous sublayer is given by $\epsilon = 2\nu(\partial k^{1/2}/\partial x)^2$ (Ref. 17). By assuming a parabolic distribution of $k$ in the viscous sublayer, $k = k_v(x/x_v)^2$, the expression for $\epsilon$ inside the viscous sublayer is obtained as $\epsilon = 2\nu k_v / x_v^2$.

In the turbulent region, by assuming linear variation of $k$ with distance from the wall beyond the edge of the viscous sublayer (Fig. 3), the expression $\epsilon = C_\mu^{3/4} k^{3/2} / \kappa x$ (Ref. 18) is integrated. By including the contribution of dissipation in the viscous sublayer, the Table 2 expression for $(\rho\epsilon)_{P,w}$ is obtained.

*Wall Shear Stress*

The present near-wall model differs importantly from the original form of Chieng and Launder in that $\tau_w$ is determined using the turbulent kinetic energy at the grid node next to the surface $k_P$, not at the edge of visocus sublayer $k_v$. Profiles of shear stress and heat transfer along the surface are very sensitive to this modification. The improvement in accuracy with this modified modeling of the near-wall flow has been reported.[19]

*Wall Shear Stress with Throughflow*

To account for throughflow at the impingement surface, the expression for wall shear stress must be modified to include the effect of mass transfer at this boundary. This is accomplished in the following way. With $u_s \, \partial v / \partial x$ much greater than $v \, \partial v / \partial y$ in the neighborhood of the wall, the boundary-layer equation becomes

$$u_s \frac{\mathrm{d}v}{\mathrm{d}x} = \frac{1}{\rho} \frac{\mathrm{d}\tau}{\mathrm{d}x}$$

By substitution of the Prandt's mixing length hypothesis, $\tau = \rho \kappa^2 x^2 (\mathrm{d}v/\mathrm{d}x)^2$, and solving for $v$, the following bilogarithmic expression is obtained:

$$v^+ = A + B \, \ell n x^+ + \frac{1}{4\kappa^2} \frac{u_s}{v\tau} \ell n^2 x^+ \tag{3}$$

where $A$ and $B$ are constants, and $v_\tau = \tau_w / \rho C_\mu^{1/4} k_P^{1/2}$.

**Table 2 Summary of equations of near-wall model[a]**

$k$ Equation:

Generation:

$$G_{P,w} = \left\{ \frac{\tau_w(v_e - v_v)}{x_e} + \frac{\tau_w(\tau_e - \tau_w)}{\rho\kappa C_\mu^{1/4} k_v^{1/2} x_e}\left(1 - \frac{x_v}{x_e}\right) + \left[ \tau_w\left(1 - \frac{x_v}{x_e}\right) + \frac{1}{2}(\tau_e - \tau_w)\left(1 - \frac{x_v}{x_e}\right)^2 \right] \left.\frac{\Delta u}{\Delta y}\right|_P + 2\mu_T \left[ \left( \left.\frac{\Delta u}{\Delta x}\right|_P \right)^2 + \left( \left.\frac{\Delta v}{\Delta y}\right|_P \right)^2 \right] \right\} \Delta x_{We}\, \Delta y_{ns}$$

Dissipation:

$$(\rho\epsilon)_{P,w} = \left\{ \frac{2C_\mu^{1/4} k_v^{3/2}}{11.5 x_v} + \frac{C_\mu^{3/4}}{\kappa x_e}\left[ \frac{2}{3}(k_e^{3/2} - k_v^{3/2}) + 2a(k_e^{1/2} - k_v^{1/2}) + b \right] \right\} \rho \Delta x_{We}\, \Delta y_{ns}$$

where

$$\tau_w = \mu_T \left( \frac{\partial u}{\partial y} + \frac{\partial v}{\partial x} \right); \qquad x_v = \frac{11.5\nu}{C_\mu^{1/4} k_v^{1/2}}; \qquad a = k_P - \frac{k_P - k_E}{x_P - x_E} x_P$$

and where

$$b = \begin{cases} \text{if } a > 0 & a^{3/2}\, \ell n \left[ \dfrac{(k_e^{1/2} - a^{1/2})(k_v^{1/2} + a^{1/2})}{(k_v^{1/2} - a^{1/2})(k_e^{1/2} + a^{1/2})} \right] \\ a = 0 & 0 \\ \text{if } a < 0 & 2(-a)^{3/2} \left( \tan^{-1} \dfrac{k_e^{1/2}}{(-a)^{1/2}} - \tan^{-1} \dfrac{k_v^{1/2}}{(-a)^{1/2}} \right) \end{cases}$$

Wall shear stress:

Without throughflow:

$$\tau_w = \kappa C_\mu^{1/4}\, \rho v_P k_P^{1/2} / \ell n(E x^+)$$

With throughflow:

$$\tau_w = \kappa C_\mu^{1/4}\, \rho v_P k_P^{1/2} \Big/ \left[ \ell n(E x^+) - \frac{u_s}{4\kappa C_\mu^{1/4} k_P^{1/2}}\, \ell n^2(x^+) \right]$$

where

$$x^+ = \frac{C_\mu^{1/4} \rho x_P k_P^{1/2}}{\mu_L}; \qquad E = 9; \qquad \kappa = 0.4$$

$\epsilon$ Equation:

$$\epsilon_P = \frac{C_\mu^{3/4} k_P^{3/2}}{\kappa x_P}$$

Energy equation:

$$St = \frac{-\dot{q}_w}{(h_P - h_w)\rho v_P} = \frac{\tau_w / \rho v_P^2}{\sigma_T [1 + P(\tau_w / \rho v_P^2)^{1/2}]}; \qquad P = 9[(\sigma_L/\sigma_T) - 1](\sigma_L/\sigma_T)^{-1/4}$$

where $\sigma_L = 0.7$ and $\sigma_T = 0.9$

[a]Refer to Fig. 3 for nomenclature.

Theoretically, $A$ and $B$ should be functions of the throughflow velocity $u_s$ (Ref. 24), and their values for the limiting case of no-throughflow $u_s = 0.0$, should logically be related to the constants of the log law of the wall, $A = \ell nE/\kappa$ and $B = 1/\kappa$. In an attempt to find $A$ and $B$ in terms of $u_s$, use of the data of Favre et al.[20] indicated that $B$ does not vary appreciably with throughflow, whereas $A$ displays a maximum,[13] with the values calculated for $u_s = 0.0$ being different from those obtained from the preceding relations. However, the average value of $B$ was found to be 2.5, which equals the inverse of the von Kármán constant, $\kappa = 0.4$. Because of the lack of detailed measurements, as the best approximation, $A$ was chosen in such a way that the constant $E$ in the log law of the wall retained its original value of 9 for smooth, nontranspiring walls.

## Numerical Procedure

### Finite-Difference Solution

Of the two common alternatives for the solution of finite-difference equations, the upwind and hybrid schemes,[16] the former yields better computational economy and stability and faster convergence. However, a numerical error, "false diffusion," may occur where the streamlines are not perpendicular to the grid lines. In the stagnation region small grid meshes were used to accommodate the steep velocity gradients. As a test, a single impinging jet case was solved with both the hybrid and upwind schemes. Since the difference in Nusselt number profiles was everywhere less than 2%, a negligible error of the false diffusion type was thereby demonstrated. The higher under-relaxation necessary with the hybrid scheme

slows the convergence rate considerably. In the present case various factors contribute to making the false diffusion error negligible, as detailed by Patankar[14] and Polat.[13]

The code 2/E/Fix of the CHAMPION series developed by Pun and Spalding[21] was modified for use in the present work.

#### Grid Layout and Grid Independent Results

A combination of uniform and nonuniform rectangular grid size achieved accuracy with minimum computational time.[13] In the $y$ direction, from the jet symmetry line to the nozzle corner and for multiple jets from the exhaust corner to the exhaust symmetry line, a uniform grid spacing was used. The nozzle and exhaust port walls coincided with a control volume boundary. Downstream of the nozzle an expanding $y$ direction grid layout (factor 1.05–1.1) was adopted. In the $x$ direction the grid layout was uniform.

The following observations result from extensive tests with the number and distribution of grids, performed to obtain grid-independent results. High aspect ratio meshes (as high as 35) in the wall jet region were proven acceptable. The nondimensional distance $x^+$ from the impingement surface to the first grid line is an important parameter because the latter must be within the fully turbulent regime, as discussed earlier. When the nondimensional distance of the grid next to the wall was between 80 and 200, the shear stress and Nusselt number profiles at the surface were found to be grid independent, as defined by a maximum deviation of 5% at the off-stagnation maximum of the Nusselt number profile. Centerline velocity decay and surface pressure profiles are less dependent on this near-wall grid spacing. Within the jet nozzle at least five grid lines in the half-nozzle width are required for grid-independent results. At the maximum $Re$ of 44,300, decreasing the number of grid nodes from 1000 (25 × 40) to 600 (20 × 30) caused a maximum difference of only 3% in local Nusselt number. The number of grid nodes required for results to be grid independent increased with increasing values of $Re$ as well as with the dimensions in the $x$ and $y$ directions. All results reported here are thus grid independent according to the criteria noted earlier.

## Results for Single-Jet Heat Transfer

The demonstration by Polat[13] that the present numerical model predicts accurately the heat transfer distribution under a single turbulent jet impinging on an impermeable surface suggested testing its ability to predict the effects of nozzle-exit turbulence and impingement surface throughflow, two parameters known to enhance heat transfer greatly.

#### Effect of Nozzle-Exit Turbulence

The extent to which convective transfer rate is increased by increasing turbulence at the nozzle exit remains an important question in impingement heat transfer. For $H/w = 2$ and $Re_j = 11{,}000$, Fig. 4 compares the predicted effect of jet inlet turbulence intensity on $Nu$ profiles with the experimental results of Gardon and Akfirat.[22] In these runs the number of grid nodes was 12 (uniform) × 35 (expanding with a factor 1.05).

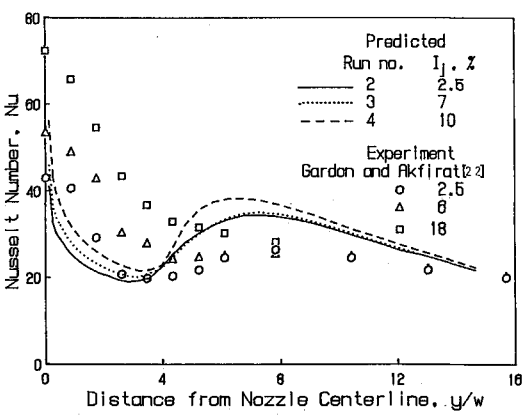


**Fig. 4 Effect of nozzle-exit turbulence intensity on profiles of local Nusselt number; $Re_j = 11{,}000$, $H/w = 2$.**

The reasons for an off-stagnation minimum and maximum at $H/w$ spacings less than 8 was ascribed by Gardon and Akfirat to boundary-layer transition. The minima in $Nu$ profiles reflect the end of the growth of a purely laminar boundary layer from its minimum thickness at the stagnation point. The increase in heat transfer beyond the minima is due to the enhanced transport characteristics of a boundary layer in transition to turbulence. Beyond the off-stagnation maxima, $Nu$ profiles decline again with growth of the turbulent boundary layer. For $H/w < 8$, Gardon and Akfirat reported that by using screens to increase the turbulence level at the nozzle exit, the heat transfer was increased, mostly in the stagnation region, but was increased substantially even out to $8w$ from the nozzle centerline. A similar observation was made by Saad,[23] who varied turbulence intensity at the nozzle exit by varying the width of slot nozzles over the range 2.5–13.3 mm.

Over the region of greatest sensitivity, $4 < y/w < 9$, the present predictions show a curious nonlinearity in that, as nozzle-exit turbulence intensity is increased from 2.5 to 7%, $Nu$ is unaffected, but when exit turbulence intensity increased further to 10%, $Nu$ increases by 10–15%. In the stagnation region Gardon and Akfirat's measurements for the same $H/w$ and $Re$ show a strong, continuous effect of nozzle-exit turbulence level for their values of 2.5, 6, and 18%. For 18% turbulence no profile of Nusselt number could be predicted because of convergence problems. The increase in stagnation region heat transfer measured by Gardon and Akfirat was so large that by 6% turbulence intensity the off-stagnation minimum becomes simply a plateau. With 18% turbulence the $Nu$ profile they measured decreases smoothly from the stagnation-point peak to a value of $Nu$ at $y/w = 8$, which, without turbulence enhancement, would be that of the secondary peak. The phenomenon of boundary-layer transition from laminar to turbulent is beyond the ability of the present turbulence[16] and near-wall models.[19] With the modeling used here for turbulent kinetic energy and near-wall shear stress, prediction of the off-stagnation minimum and secondary maximum in Nusselt number profiles is therefore purely coincidental. No near-wall model[4,6,19] is able to simulate the phenomena that create these off-stagnation features, namely, boundary-layer transition from laminar at the end of the stagnation region to turbulent at the off-stagnation maximum. The underprediction by the present model of the effect of nozzle-exit turbulence on heat transfer may also derive from the inability of the $k$-$\epsilon$ turbulence model to simulate the actual anisotropy of turbulence in stagnation flows.

#### Effect of Impingement Surface Throughflow

*Effect on Heat Transfer*

The values of $Re_j$, $H/w$, and throughflow rates, listed in Table 3, were selected to duplicate those for which heat-transfer rates have been measured.[13] The nozzle-exit turbulence intensity used, 7% is within the range where the model is insensitive to this parameter (Fig. 4).

**Table 3 Parameter values for single-jet simulations with throughflow at the impingement surface, $H/w = 2.5$, $I_j = 7\%$**

| Run no. | $Re_j$ | $NX$ | $NY$ | $u_s$, m/s | $Mu_s = u_s/u_j$ |
|---|---|---|---|---|---|
| 6 | 21,800 | 15 | 30 | 0.0 | 0.0 |
| 11 | 21,800 | 15 | 30 | 0.094 | 0.0044 |
| 12 | 21,800 | 15 | 30 | 0.256 | 0.012 |
| 7 | 35,800 | 20 | 30 | 0.0 | 0.0 |
| 13 | 35,800 | 20 | 30 | 0.109 | 0.0032 |
| 8 | 44,300 | 25 | 40 | 0.0 | 0.0 |
| 14 | 44,300 | 25 | 40 | 0.095 | 0.0023 |
| 15 | 44,300 | 25 | 40 | 0.237 | 0.0058 |

Relative to the no-throughflow case, the model predicts a uniform increase in $Nu$ along the impingement surface with application of uniform throughflow, exactly as is measured experimentally.[13,23] A comparison with measured heat transfer rates (Fig. 5) is therefore made on the previously established basis, i.e., as an enhancement of the average Stanton number due to throughflow, $\Delta\overline{St}$, relative to the nondimensional measure of throughflow, $Mu_s$. The second feature documented experimentally[13] is that $\Delta\overline{St}/Mu_s = 0.175$, independent of $Mu_s$, $Re_j$, and $S/w$. When the predicted results at $S/w = 8$ are cross plotted with respect to $Mu_s$, the ratio $\Delta\overline{St}/Mu_s$ is seen to increase with $Mu_s$ rather than to be independent of $Mu_s$. As $Mu_s \to 0$, the predicted $\Delta\overline{St}/Mu_s$ approaches the experimentally measured value, 0.175. Within the range $0 < Mu_s < 0.002$ the predicted enhancement ratio $\Delta\overline{St}/Mu_s$ agrees within 10% of that measured experimentally,[13] but for $Mu_s > 0.002$ the model overpredicts the enhancement in average heat transfer by throughflow. This limitation is not of much importance because the range $Mu_s \leq 0.002$ covers throughflow rates of particular interest for industrial application.

Various effects are responsible for the disagreement between the predicted and experimental values of $\Delta\overline{St}/Mu_s$ in the stagnation region. Complete isotropy of flow, assumed by the turbulence model, fails in this region. The assumptions of Couette flow and of equilibrium between turbulent kinetic energy generation and dissipation for $\tau_w$ expressions (Table 2) also fail. Moreover, very near the stagnation point the predicted $Nu$ profiles decay faster due to the choice of separate modeling of near-wall flow. The value defined as stagnation-point $Nu$ is actually computed at the grid node next to the true stagnation point; hence, its value is very sensitive to the location of this node because $\tau_w$ and $v_P$ both approach zero as the true stagnation point is approached.

The reason why predicted $\Delta\overline{St}/Mu_s$ increases with $Mu_s$ is probably the fixed values of $A$ and $B$ used in the bilogarithmic formula, Eq. (3), used to calculate wall shear stress in the case with throughflow. Although $A$ and $B$ in the $\tau_w$ equation for throughflow should depend on throughflow velocity,[24] the values for the no-throughflow case were used. Attempts to correlate $A$ and $B$ with $u_s$, using the boundary-layer velocity-throughflow measurements of various studies, especially that of Favre et al.,[20] were unsuccessful due to limitations in the experimental data. Until more accurate studies appear, this problem restricts the maximum throughflow rate for which the model may be used.

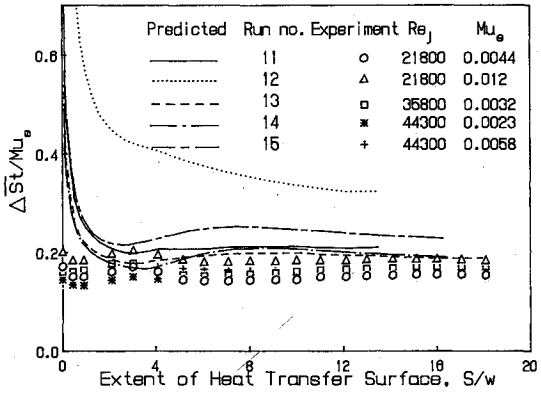


**Fig. 5 Profiles of enhancement of average Stanton number.**

*Effects on the Flowfield*

Since the model gives a remarkably good prediction of heat transfer enhancement except for very high throughflow, several of the predicted effects of throughflow on the flow are now examined, specifically, the effects on axial velocity near the impingement surface (Fig. 6), on profiles of lateral velocity (Fig. 7), and on turbulent kinetic energy very close to the impingement surface (Fig. 8).

For $H/w = 2.5$ the predicted lateral profiles of axial velocity at positions, $H-x$, of $0.5w$ ($0.2H$) and $0.1w$ ($0.04H$) from

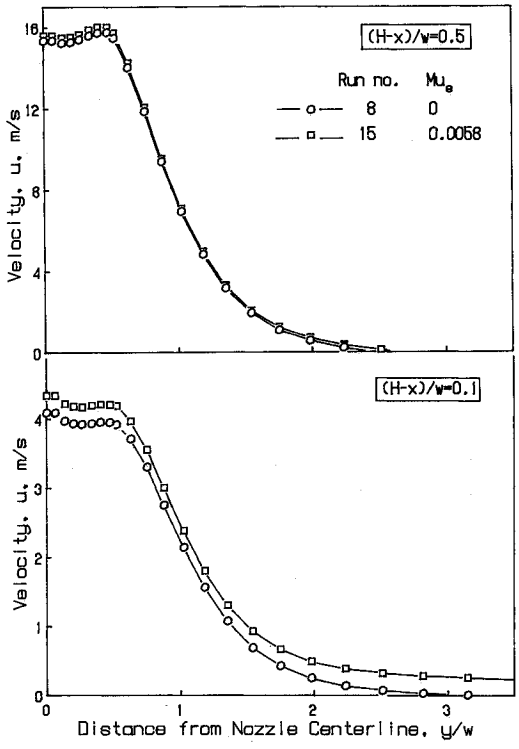


**Fig. 6 Effect of throughflow at the impingement surface on lateral profiles of axial velocity at $0.5w$ and $0.1w$ from the impingement surface; $Re_j = 44{,}300$, $u_j = 42$ m/s, $H/w = 2.5$.**

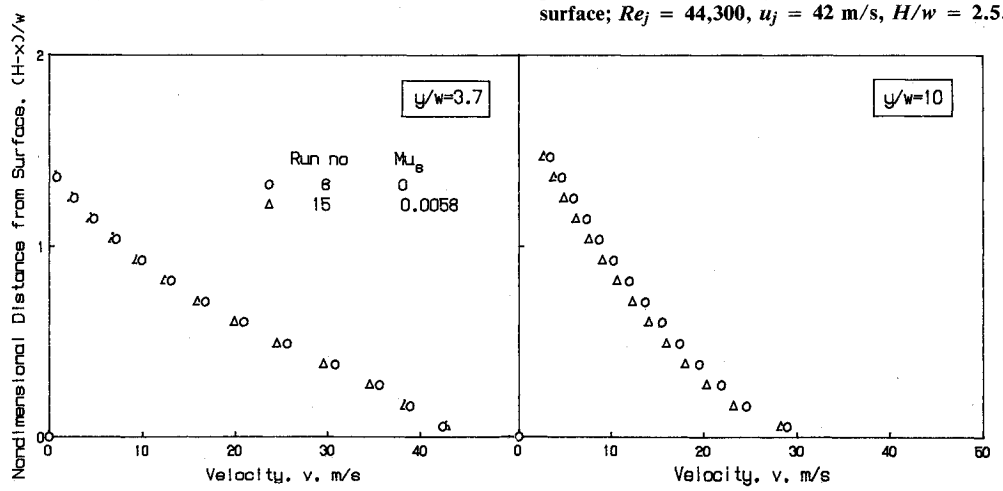


**Fig. 7 Effect of throughflow at the impingement surface on profiles of lateral velocity; $Re_j = 44{,}300$, $H/w = 2.5$.**

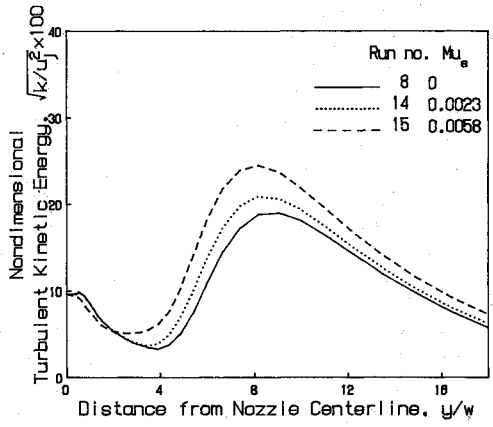


**Fig. 8 Effect of throughflow at the impingement surface on profiles of turbulent kinetic energy near impingement surface; $Re_j$ = 44,300, $H/w$ = 2.5.**

the impingement surface (Fig. 6) show almost no effect of throughflow even as close as $0.5w$ from the surface. At $0.1w$ from the impingement surface, throughflow increases axial velocity by an almost uniform amount everywhere, with the relative increase becoming very large by even $1.5w$ from the nozzle centerline. For a confined slot and an unconfined round jet, respectively, Saad[23] and Obot[25] measured these profiles at a position $2w$ ($0.25H$) from the surface when the impingement surface was spaced $8w$ from the nozzle. Saad's measurements show that, at a uniform throughflow velocity of 0.3 m/s, axial velocity increased by a constant amount everywhere, independently of $Re_j$ (11,000 < $Re_j$ < 30,000). At a jet Reynolds number of 38,000 and for a uniform $u_s$ of 0.175 and 0.25 m/s, Obot observed the same effect. Contrary to those measurements, the present predictions show a negligible effect of throughflow on axial velocity at $0.2H$ from the impingement surface.

The Fig. 7 comparison of predicted profiles of lateral mean velocity across the wall jet, with and without throughflow, indicates a negligible effect out to $3.7w$ from stagnation. By $10w$ from stagnation, the prediction is for lateral velocity near the impingement surface to decrease slightly, by 5%. For $Mu_s$ = 0.0058 the cumulative amount of air removed by throughflow out to $y/w = 10$ is 12% of the jet inflow. The measurements of Saad[23] and Obot[25] indicate that throughflow increases the streamwise velocity near the surface, as did the measurements of Baines and Keffer[26] for an unconfined slot jet impinging at a fixed $u_s/u_j$ value of 0.29%. Thus, the predicted effect is opposite to three experimental observations. Limitations of the turbulence model may be a factor. It is well known that the distance from the impingement surface for the positions of zero shear stress and of maximum wall jet velocity do not coincide. How throughflow affects this relationship is unknown. A turbulent-viscosity model such as that used here cannot predict the correct location of the wall jet velocity maximum because it implicitly requires the zero shear stress and velocity maximum to be coincident. Moreover, when a high-$Re$ version turbulence model is used, near-wall properties such as wall shear stress and heat transfer are estimated using wall functions, with the consequence that detailed features of the near-wall flow are not simulated.

Since Saad[23] also found that throughflow did not affect axial turbulence velocity, his axial turbulence intensity decreased with throughflow. For a round jet Obot[25] found the same effects for both axial and streamwise turbulence. In Fig. 8 the predicted nondimensional turbulent kinetic energy profiles along the grid line next to the impingement surface, i.e., about $0.1w$ from it, are displayed for the same throughflow rates as those of Fig. 7. Thus, beyond the impingement region the numerical model predicts a decrease in near-wall lateral velocity (Fig. 7), accompanied by an increase in turbulent kinetic energy near the surface (Fig. 8). Both trends are opposite to the measurements of Saad and Obot. Within throughflow rates of industrial relevance the model therefore predicts about the correct enhancement in average heat transfer by throughflow (Fig. 5), but paradoxically, the mechanisms by which the model does this are not consistent with the experimental evidence (Figs. 6–8).

**Table 4 Parameter values for multiple-jet simulations**

| Run no. | $H/w$ | $Re_j$ | $I_j$,% | $NX$ | $NY$ | $S/H$ | $u_s$, m/s | $Mu_s$, $= u_s/u_j$ |
|---|---|---|---|---|---|---|---|---|
| 16 | 8 | 21,000 | 1 | 25 | 30 | 1.0 | 0 | 0 |
| 17 | 8 | 21,000 | 1 | 25 | 30 | 0.75 | 0 | 0 |
| 18 | 8 | 21,000 | 1 | 25 | 30 | 0.5 | 0 | 0 |
| 19 | 8 | 21,000 | 1 | 25 | 30 | 0.375 | 0 | 0 |
| 20 | 5 | 8,200 | 5 | 20 | 25 | 0.5 | 0 | 0 |
| 21 | 5 | 8,200 | 5 | 20 | 25 | 0.5 | 0.043 | 0.0031 |
| 22 | 5 | 8,200 | 5 | 20 | 25 | 0.5 | 0.109 | 0.0079 |
| 23 | 5 | 8,200 | 5 | 20 | 25 | 0.5 | 0.161 | 0.0117 |
| 24 | 5 | 8,200 | 5 | 20 | 25 | 0.5 | 0.268 | 0.0194 |

## Multiple-Jet Heat Transfer With and Without Throughflow

The model was used to predict heat transfer for a multiple confined jet configuration with exhaust ports located symmetrically between the jet nozzles (Fig. 2). The width of exhaust ports is twice that of the jet nozzles. For such a multiple-jet system composed of repeating units, or flow cells, of dimensions $S \times H$, Saad[23] established that flow cell aspect ratio $S/H$ is a basic parameter that defines conditions of geometric similarity for flow and heat transfer. Because of flow symmetry, only the domain of a single flow cell, $S \times H$, needs to be solved. Figure 2 indicates that each such flow cell takes half of the flow from a nozzle. Since the only comparable experimental data are those by Saad without throughflow, and those of Polat[13] with and without throughflow, two series of simulation runs were made (Table 4), one matching the conditions of each of these experimental studies.

### Heat Transfer Profiles

Since Saad[23] measured local Nusselt number profiles for multiple confined slot jets at $Re_j = 21{,}000$, $H/w = 8$ for flow cell aspect ratio $S/H$ of 1 and 0.75, the model was used to predict $Nu$ for these conditions. Two lower values of $S/H$, 0.5 and 0.375, were added to provide results for closely spaced nozzles and exhaust ports. In these simulations $H$ and $w$ were fixed, and the variation in $S/H$ from 1 to 0.375 was obtained by changing the nozzle-to-exhaust port spacing, $S$. The number of grid nodes was fixed at 25 × 30, and the nozzle-exit turbulence instensity was fixed at 1%. Saad used elliptically contoured entry nozzles in his multiple-jet study, for which he measured nozzle-exit turbulence intensities of less than 1%. Because the present model is insensitive to nozzle-exit turbulence intensities of 2.5–7% even for a spacing as small as $H/w$ = 2 (Fig. 4), the choice of 1% intensity is reasonable.

The sharp increase in predicted $Nu$ with approach to within about $0.25w$ of the centerline of both the exhaust port and the jet nozzle (Fig. 9) is the same characteristic apparent very near the nozzle centerline for the single-jet profiles (Fig. 4). As described earlier, the inability of the simulation to predict $Nu$ satisfactorily within about $0.25w$ of the jet and exhaust flow centerlines is attributed to the wall function method used.

Over the central 80% of the nozzle-to-exhaust port spacing $S$, Fig. 9 shows that the agreement between $Nu$ predicted and $Nu$ measured by Saad is within 30% for $S/H$ of 1 and 0.75. Saad reported an uncertainty of less than 10% for those measurements. No experimental data exist for $S/H$ of 0.5 and 0.375. From his measurements over a wide range of $S/H$ at larger values of $H/w$, Saad predicted that the average heat transfer rate at any $H/w$ would pass through a maximum value for a flow cell aspect ratio around $S/H$ = 0.5. The Fig. 9 results indicate that the heat transfer rate increases as $S/H$ is decreased from 1 to 0.75 to 0.5. For $S/H$ = 0.375, i.e., $S/w$

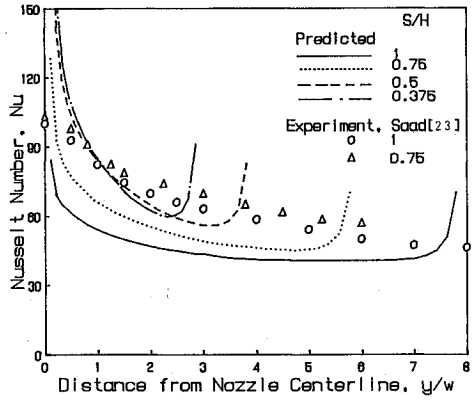


**Fig. 9 Effect of jet-to-exhaust spacing, $S/H$, on profiles of local Nusselt number in a multiple-jet system; $Re_j$ = 21,000, $H/w$ = 8.**

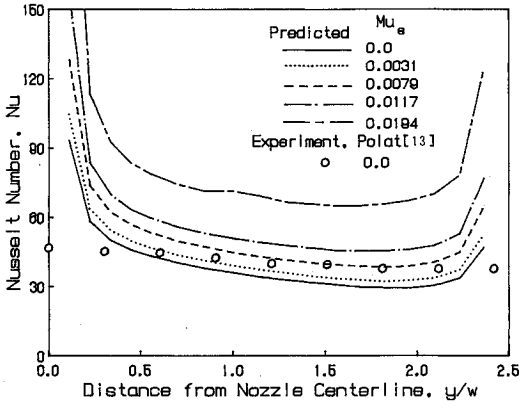


**Fig. 10 Effect of throughflow at the impingement surface on profiles of local Nusselt number in a multiple-jet system; $Re_j$ = 8200, $H/w$ = 2.5, $S/H$ = 0.5.**

= 3, the simulation predicts a lower $Nu$ over the central region $1 < y/w < 2.5$ for which the simulation is not distorted by the near-centerline problem discussed earlier. Thus, the simulation model is consistent with the experimentally based prediction of Saad that $\overline{Nu}$ passes through a maximum for a spacing of about $S/H = 0.5$.

The effect of throughflow on multiple-jet impingement heat transfer was predicted in a second set of runs at $S/H = 0.5$, $H/w = 5$, and with the other conditions corresponding to available measurements.[13] In these runs the number of grid nodes was 20 × 25, and the nozzle-exit turbulence intensity was 5%. For the case without throughflow Fig. 10 displays the predicted and experimental $Nu$ profiles. For a flow cell this narrow, the two critical regions with anisotropic characteristics, i.e., the impingement and exit flows, are very close. The prediction of such a flow configuration with a turbulence model that assumes isotropy is expected to be less satisfactory. However, agreement between experimental and predicted $Nu$ profiles is surprisingly good, within 15% over the central 80% of the impingement surface, $0.25 < y/w < 2.25$, i.e., excluding the two near-centerline regions for which the model is never reliable.

### Average Heat Transfer

The predicted effect of throughflow (Fig. 10), like that measured experimentally, is for local enhancement of heat transfer by an almost uniform amount across the impingement surface, excluding the 10% of the surface adjacent to the two centerlines, where, as discussed, the simulation is invalid. For the average heat transfer comparison of Fig. 11, the predicted values of $\overline{Nu}$ were calculated by excluding the region of invalid predictions within $0.25w$ of the nozzle and exhaust port centerlines. The agreement between predicted and measured average heat transfer with throughflow, good for $Mu_s$

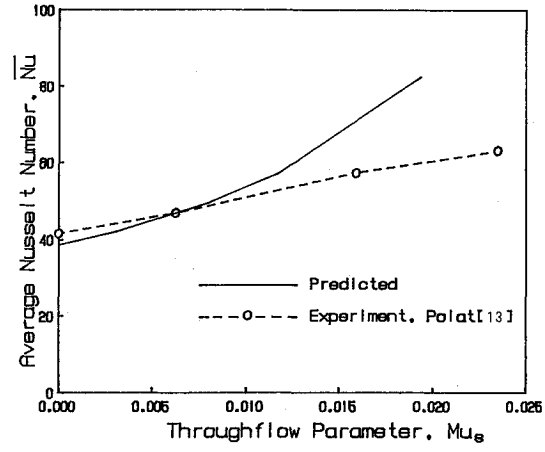


**Fig. 11 Effect of throughflow at the impingement surface on average Nusselt number in a multiple-jet system; $Re_j$ = 8200, $H/w$ = 2.5, $S/H$ = 0.5.**

< 0.01, becomes much too high at higher $Mu_s$ for the reasons noted in the single-jet case. Hence, for such a multiple-jet system this near-wall model can be used only for values of the throughflow parameter, $Mu_s$, smaller than 0.01. For a single jet the upper limit on throughflow rates for which the model gives good predictions of the heat transfer enhancement by throughflow is much smaller yet, about $Mu_s = 0.002$. However, because the simulations for the single jet were performed at much higher jet Reynolds numbers, 22,000–44,000, this limiting value of $Mu_s$ for a single jet corresponds to a throughflow velocity $u_s$ about the same as that for the multiple jets at $Re_j = 8200$ and $Mu_s = 0.01$, i.e., $u_s \simeq 0.1$ m/s in both cases. This value is within the range of throughflow velocities achieved in experiments with the proposed combined impingement and through dryer for paper,[13] $0.05 < u_s < 0.27$ m/s.

The tests performed thus establish that, for multiple confined slot jets, the present model predicts Nusselt number to within 30% of that measured experimentally and shows trends close to those observed for the effect of internozzle spacing $S/H$ and for the effect of the throughflow up to industrially relevant values of $u_s$.

## Summary

Flow and heat transfer under confined turbulent impinging slot jets were predicted by solving iteratively the two-dimensional Navier-Stokes, energy, and the turbulence model equations. The turbulence model used was the high-Reynolds-number version of the well-known $k$-$\epsilon$ model. The near-wall model used was of the Chieng-Launder type, as modified by Polat et al.[19] The predictive capability of this numerical technique was tested for the effects of nozzle-exit turbulence and of surface throughflow for a single jet and for the industrially important case of a confined system of multiple jets with symmetrical exhaust ports with and without throughflow.

When turbulence intensity at the nozzle exit is increased for small nozzle-to-surface spacings, the model fails to predict the enhancement of impingement heat transfer observed experimentally out to about $8w$ from stagnation. This deficiency relates to the inability of the technique to predict the boundary-layer phenomena involved in that enhancement.

The prediction of enhancement of heat transfer by throughflow at the impingement surface according to this model is accurate to within 10% for practical rates of throughflow, $Mu_s < 0.002$, for the single jet. For higher throughflow rates, the model substantially overpredicts the enhancement. The source of this error is probably that, due to a lack of studies on the effect of throughflow on the near-wall flow, the parameters of the bilogarithmic formula used for wall shear stress cannot be related to throughflow rate.

For the case of a confined multiple-jet configuration with exhaust ports located symmetrically between the jets, the pre-

dicted *Nu* profile is as much as 30% lower than that measured. When the nozzle centerline-to-exhaust centerline spacing *S* was varied, the model results indicate that an average *Nu* passes through a maximum near the same value of the flow cell aspect ratio, $S/H = 0.5$, as was indicated by the experimental measurements of Saad.[23] The predicted effect on heat transfer of throughflow at the impingement surface agrees quite well with experimental measurements for values of the throughflow parameter up to $Mu_s = 0.01$, beyond which the model overpredicts the enhancement, as for a single jet. The limiting value of $Mu_s$ for good agreement between predicted and experimental results for the effect of throughflow is quite different for single and multiple jets, but, interestingly, the throughflow velocities corresponding to these limiting values of $Mu_s$ are about the same, $u_s \simeq 0.1$ m/s.

In conclusion, the enhancement of convective heat transfer due to throughflow at the impingement surface can be predicted with reasonable accuracy up to substantial throughflow rates of 0.1 m/s but is overpredicted at higher throughflow. The model does not predict the heat transfer enhancement with increasing nozzle-exit turbulence which has been measured. This technique, which incorporates a high-*Re* version of the $k$-$\epsilon$ model with a modified Chieng-Launder-type near-wall model, thus lacks the accuracy and generality that is sought for numerical prediction methods. The use of a more detailed turbulence model may be justified in view of the complex turbulence structure of a confined impinging jet system. Such models, not yet adequately tested, are still in the development stage. Prediction of heat transfer under impinging jets remains a particularly stringent test for the performance of any such turbulence model.

## References


[1]Folayan, C. O., "Impingement Cooling," Ph.D. Dissertation, Imperial College, London, 1977.

[2]Guo, C. Y., and Maxwell, W. H. C., "Numerical Modeling of Normal Turbulent Plane Jet Impingement on a Solid Wall," *Journal of Engineering Mechanics,* Vol. 110, No. 10, 1984, pp. 1498–1509.

[3]Huang, G. P., Mujumdar, A. S., and Douglas, W. J. M., "Numerical Prediction of Fluid Flow and Heat Transfer Under a Turbulent Impinging Slot Jet with Surface Motion and Crossflow," *American Society of Mechanical Engineers,* Paper 84-WA/HT-33, 1984.

[4]Polat, S., Mujumdar, A. S., and Douglas, W. J. M., "Heat Transfer Distribution Under a Turbulent Impinging Jet," *Drying Technology,* Vol. 3, No. 1, 1985, pp. 15–38.

[5]Polat, S., Mujumdar, A. S., and Douglas, W. J. M., "Numerical Prediction of Multiple Impinging Turbulent Slot Jets," *Drying '86,* edited by A. S. Mujumdar, Hemisphere, New York, 1986, pp. 853–864.

[6]Van Heiningen, A. R. P., "Heat Transfer Under an Impinging Slot Jet," Ph.D. Dissertation, McGill Univ., Montreal, 1982.

[7]Van der Meer, T., "Heat Transfer from Impinging Flame Jets," PhD Dissertation, Delft University, Delft, the Netherlands, 1987.

[8]Looney, M. K., and Walsh, J. J., "Mean Flow and Turbulent Characteristics of Free and Impinging Jet Flows," *Journal of Fluid Mechanics,* Vol. 147, 1984, pp. 397–429.

[9]Rodi, W., Ph.D. Dissertation, Univ. of London, 1972.

[10]Ljuboja, M., and Rodi, W., "Calculation of Turbulent Wall Jets with an Algebraic Stress Model," *Proceedings of a Symposium on Turbulent Boundary Layers: Forced, Incompressible, Non-Reacting,* edited by H. E. Weber, 1979, pp. 131–138.

[11]Polat, S., Huang, B., Mujumdar, A. S., and Douglas, W. J. M., "Numerical Flow and Heat Transfer Under Impinging Jets—A Review," *Annual Review of Numerical Fluid Mechanics and Heat Transfer,* Vol. 2, Hemisphere, New York, 1989, pp. 157–197.

[12]Amano, R. S., and Sugiyama, S., "An Investigation on Turbulent Heat Transfer of an Axisymmetric Jet impinging on a Flat Plate," *Bulletin of JSME,* Vol. 28, No. 235, 1985, pp. 74–79.

[13]Polat, S., "Transport Phenomena Under Jets Impinging on a Moving Surface with Throughflow," Ph.D. Dissertation, McGill Univ., Montreal, 1988.

[14]Patankar, S., *Numerical Heat Transfer and Fluid Flow,* Hemisphere, New York, 1980, p. 70.

[15]Chieng, C. C., and Launder, B. E., "On the Calculation of Turbulent Heat Transport Downstream from an Abrupt Pipe Expansion," *Numerical Heat Transfer,* Vol. 3, 1980, pp. 189–207.

[16]Jones, W. P., and Launder, B. E., "The Calculation of Low-Reynolds-Number Phenomena with a Two-Equation Model of Turbulence," *International Journal of Heat and Mass Transfer,* Vol. 16, 1973, pp. 1119–1130.

[17]Pope, S. B., and Whitelaw, J. H., "The Calculation of Near-Wake Flows," *Journal of Fluid Mechanics,* Vol. 73, 1976, pp. 9–32.

[18]Spalding, D. B., "Heat Transfer from Turbulent Separated Flows," *Journal of Fluid Mechanics,* Vol. 27, 1967, pp. 97–109.

[19]Polat, S., Mujumdar, A. S., van Heiningen, A. R. P., and Douglas, W. J. M., "Effect of Near-Wall Modeling on Prediction of Impingement Heat Transfer," *Drying Technology,* Vol. 8, No. 4, 1990, pp. 705–730.

[20]Favre, A., Dumas, R., Verollet, E., and Coantic, M., "Couche Limite Turbulente sur Paroi Poreuse avec Aspiration," *Journal de Mécanique,* Vol. 5, No. 1, 1966, pp. 3–28.

[21]Pun, W. M., and Spalding, D. B., "A General Computer Program for Two-Dimensional Elliptic Flows," Imperial College, Mechanical Engineering Dept., London, Rept. HTS/76/2, 1977.

[22]Gardon, R., and Akfirat, J. C., "The Role of Turbulence in Determining the Heat Transfer Characteristics of Impinging Jets," *International Journal of Heat and Mass Transfer,* Vol. 8, 1965, pp. 1261–1272.

[23]Saad, N. R., "Flow and Heat Transfer for Multiple Turbulent Impinging Slot Jets," PhD Dissertation, McGill University, Montreal, 1981.

[24]Black, T. J., and Sarnecki, A. J., "Turbulent Boundary Layer with Suction or Injection," Aeronautical Research Council Reports and Memo, R&M 3387, 1958.

[25]Obot, N. T., "Flow and Heat Transfer for Round Turbulent Jets Impinging on Permeable and Impermeable Surfaces," PhD Dissertation, McGill University, Montreal, 1981.

[26]Baines, W. D., and Keffer, J. F., "Shear Stress Measurements for an Impinging Air Jet," *Transactions of the Technical Section, Canadian Pulp and Paper Association,* 1979, pp. 39–44.